Study on traction control in 4-wheel drive electric vehicle using a driving simulator

A. Michinao Saito[1*], B. Kantaro Yoshimoto[1], and C. Tomoki Yokoyama[1]
[1] Department of Robotics and Mechatronics, Tokyo Denki University, Tokyo, Japan

***Abstract*-- This paper proposed the maximum driving force control and evaluated MDFC with 4-wheel drive electric vehicles using a driving simulator. Maximum driving force control uses the mountain climbing method to control the torque that the driving force of the wheel can be maximized. The MDFC was evaluated on a low friction road surface in a driving simulator. The results of the slip ratio and vehicle speed showed that wheel slip was suppressed and the vehicle acceleration was improved.**

***Index Terms*-- Driving Simulator, Maximum Driving Force Control, Traction Control**

I. Introduction

In recent years, the number of fatalities in traffic accidents in Japan has been decreased compared to the 1990s. However, fatal accidents still occur due to a variety of factors. Among the environmental causes of fatal accidents involving 4-wheeled vehicles, 47 of the 121 fatal accidents, or 40% of all accidents, were caused by deteriorating road conditions(1).

Based on this problem, this paper considers the vehicle stability under various conditions like icy or wet road surfaces and the effectiveness of the traction control taking the advantage of the high response of motor control of electric vehicles. The simulated experimental environment is constructed as a simulator to demonstrate the effectiveness of the vehicle stabilization control to be studied. The traction control considered in this paper is to realize the control as an easy-to-implement control including gain tuning of the control.

II. Driving Simulator and Vehicle Model

A. Driving simulator

In this study, a driving simulator was constructed to perform vehicle driving tests in a virtual space. In the driving simulator, a head mounted display(HMD) is used to experience visually the effects of the control system constructed with Simulink. The system configuration of the driving simulator used is shown in Fig. 1. In the system flow shown in Fig. 1, PC1 loads Automotive Simulation Models (ASM), which are vehicle models built with Simulink, and their parameters from dSPACE Control Desk into the processor ds1006. After that, the processor performs the calculation and processing of those parameters. Among the calculated parameters, as vehicle spatial coordinates, vehicle angle, steering wheel rotation angle, and vehicle speed are sent from PC1 to PC2 via user datagram protocol (UDP) communication, and PC2 uses the received information to represent the current vehicle state on Unity. The driver operates the steering wheel, brake, accelerator, and gears on the driving seat based on the video information from the HMD. This operation information is obtained through ds1006 and computed again.

ASM is a tool created by dSPACE that can simulate electric vehicle motors, vehicle dynamics, electrical control systems, and traffic environments. It is a MATLAB/Simulink tool and is built on open models, making it easy to add custom models and replace existing models.

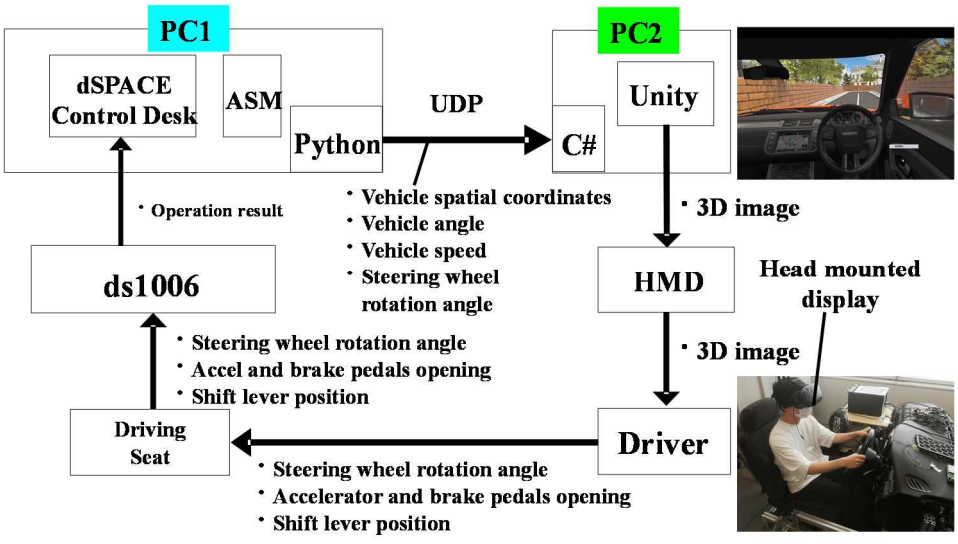

Fig.1. System configuration of the driving simulator

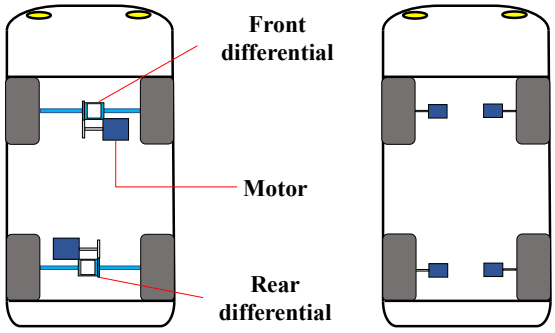

(a) Front and rear wheels independent drive (b) 4-wheel independent drive

Fig.2. Drive system for electric vehicles

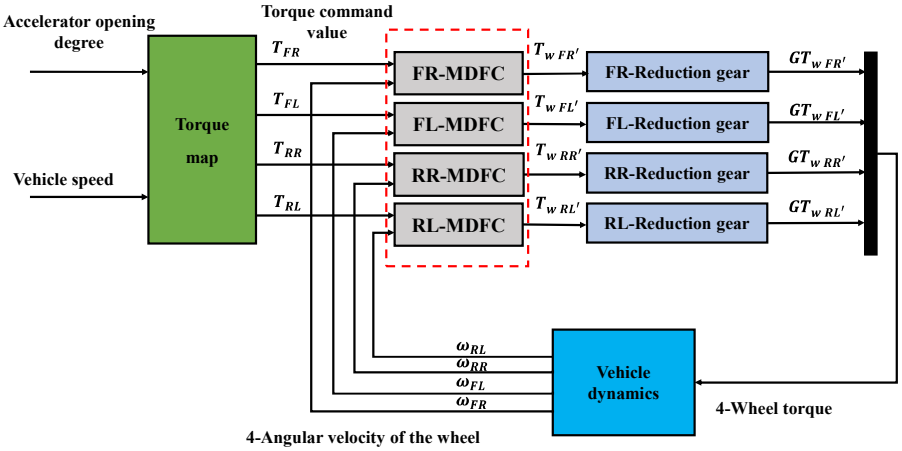

Fig.3. 4-wheel independent drive model

B. Electric vehicles to be evaluated

The drive system of the electric vehicle proposed in this is shown in Fig.2. Fig.2. (a) shows a conventional drive system for electric vehicles with independent drive for front and rear wheels. Fig.2. (b) shows a 4-wheel independent drive system. Independent drive for the front and rear wheels is a drive system currently used in commercially available electric vehicles. One motor is mounted on the front wheel side and one on the rear wheel side, and torque is output to the wheels via differential gears. A differential gear is a device that absorbs the difference between the inside and outside wheels that occurs during turning to achieve smooth turning. Therefore, the front and rear wheels can output different torques, but the left and right wheels cannot output different torques. Torque loss is also high because torque is output through the differential gear. In contrast, the 4-wheel independent drive has been proposed as a concept or a research[2][3]. Each wheel is equipped with a traction motor, then each wheel can output different torque.

C. Vehicle Model Overview

An overview of the 4-wheel independent drive vehicle model used in this study is shown in Fig.3. First, the torque map is a block that inputs the accelerator pedal position and vehicle speed and outputs a torque command value that simulates a motor. 4-wheel independent drive models have 4-motor drive, so 1/4 of the torque in the torque map is input to the control block. Next, the reduction gear block outputs the torque GT_w', which is amplified by applying the reduction ratio G. The reduction ratio is the ratio of the number of motor revolutions to the number of tire revolutions. Finally, the torque GT_w' of each wheel is calculated through vehicle dynamics, and the angular velocity ω of each of the four wheels is input to the control block. There are two types of control that will be evaluated in this study. The first is the maximum driving force control (MDFC) block, which maintains the maximum driving force and efficiently suppresses wheel spinning using the mountain climbing method. The Second is the model following control (MFC) block[4][5], reduces the torque command value when the vehicle travels on a low-friction surface and the wheels become slip, aiming for a non-spinning state.

D. Torque map simulating an electric vehicle motor

The torque characteristics of an electric vehicle motor are shown in Fig.4[6][7]. the horizontal axis is the vehicle speed [km/h] and the vertical axis is a total of traction motor torque [Nm]. The accelerator pedal opening is increased by 4% for each step increase in torque, with a minimum value of 0% and a maximum value of 100%. When the accelerator is turned off or opened at a low level, a regenerative torque command is given to improve driving operability with the accelerator pedal.

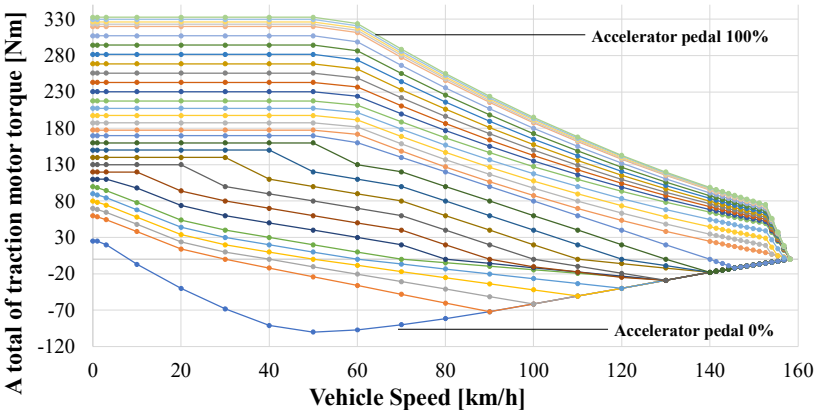

Fig.4. Torque map for a total of traction motor commanded by the accelerator pedal

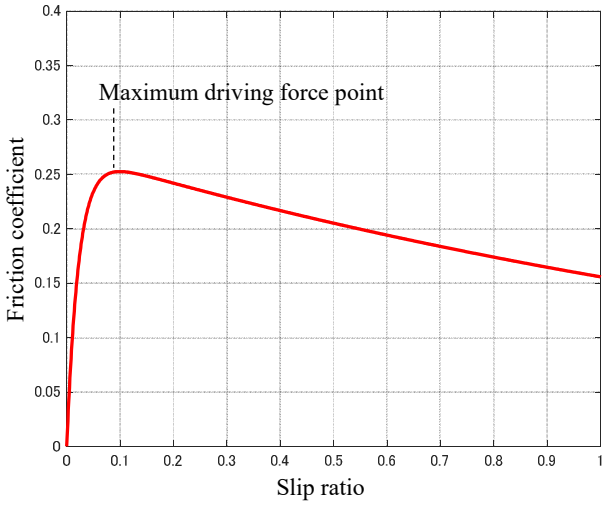

Fig.5. Friction coefficient vs. slip ratio

Table 1.

Description	Symbol	Value [unit]
Vehicle weight	M	1880 [kg]
Wheel radius	r_w	0.36 [m]
Viscosity friction	B	0 [kg · m/s]
Gear ratio (motor shaft to axle)	G	6.705
Maximum driving force gain	α	0.00001
HPF time constant	τ_{HPF}	0.002
LPF time constant	τ_{LPF}	0.25
PI time constant	τ_{PI}	0.02
Sampling time	t_d	1 [ms]

E. Maximum driving force control

The parameters used in this study are listed in Table.1. To explain maximum driving force control, first, T_w is the motor torque, μ is the friction coefficient, ω_m is the angular velocity of rotation of the motor and R is the gradient resistance. The equation of vehicle motion is shown in (1), the equation of tire (motor) rotation motion is shown in (2), and the driving force is shown in Equation [(3)(4)].

$$M\frac{dv}{dt} = F - R \tag{1}$$

$$J\frac{d\omega_w}{dt} = GT_w - r_wF - B\omega_m \tag{2}$$

$$F = \mu Mg \tag{3}$$

The relationship between driving force and slip ratio is shown in (4) for slip speed S. The slip ratio λ used to calculate the friction coefficient between the wheel and the road surface is shown in (5). Where ω_w is the wheel angular velocity and v is the vehicle body velocity.

$$S = \omega_w r_w - v \tag{4}$$

$$\lambda = \frac{v-\omega_w r_w}{v}\ (\omega_w r_w < v) \tag{5}$$

$$\lambda = \frac{\omega_w r_w - v}{\omega_w r_w}\ (\omega_w r_w > v)$$

A graph of friction coefficient vs. slip ratio is shown in Fig.5. When the slip ratio is smaller than the maximum driving force point, the traction of tire is stable condition. As the slip ratio increases, the coefficient of friction also increases. when the slip ratio is larger, the wheel slip occurs and the traction of tire is unstable. As the slip ratio increases, the coefficient of friction decreases. A block diagram of maximum driving force control is shown in Fig. 6 [(8)~(11)]. First, the slip deceleration command S_{ref} is obtained by (6), where α is maximum driving force control gain and F_{est} is the estimated driving force obtained by the disturbance observer.

$$S_{ref}(k+1) = S(k) + \alpha\frac{dF_{est}}{dS} \tag{6}$$

dF_{est}/dS is dF_{est}/dt divided by dS/dt. dF_{est}/dt and dS/dt are obtained by the quasi-derivative, respectively. dS/dt is passed through the LPF to align the time constant with F_{est}. The sum of S_{ref} and body speed v divided by the wheel radius r_w is the wheel angular velocity command ω_{ref}. The wheel angular velocity command is controlled by PI controller and compensating the disturbance from $F_{est} \cdot r_w$ as the reaction force of the driving force. and by compensating the disturbance since $F_{est} \cdot r_w$ represents the reaction force of the driving force

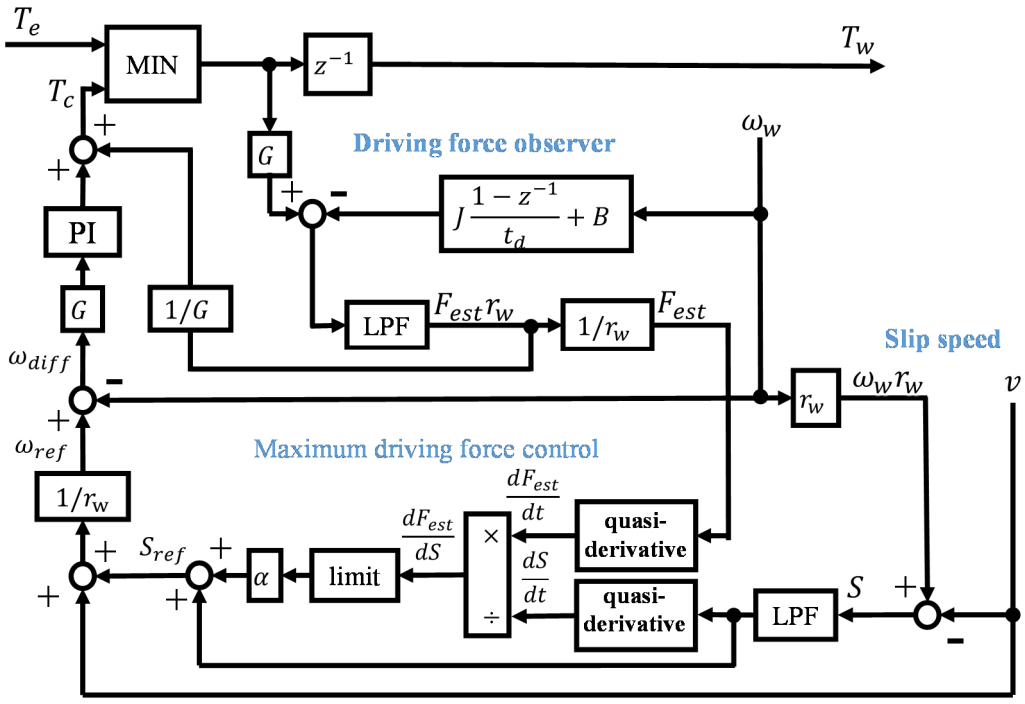

Fig.6. Maximum driving force control

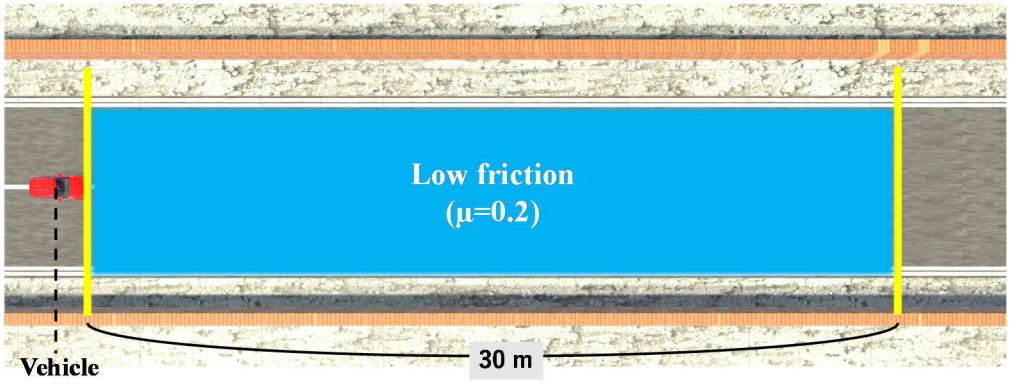

Fig.7. The course of this simulation

T_c is applied to the comparator to prevent the input torque T_e from exceeding and accelerating.

F. Simulation of driving on low friction road surfaces

The course of this simulation is shown in Fig.7. The coefficient of friction was set to 0.2 to make the low friction surface an icy road surface. In this simulation, the electric vehicle is driven straight after the start of driving. The vehicle is allowed to run for 7 s with the accelerator pedal at 100 %. On such low-friction road surfaces, the results of MDFC for the 4-wheel independent drive, are compared with those of MFC for the 4-wheel independent drive, and constant torque control for the front and rear wheel independent drive.

G. Simulation results

The obtained results are shown in Fig.8. for the body speed and 4-wheel speeds of the constant torque control, in Fig.9. for the slip ratio and in Fig.10. for the torque output of the motor. Fig.11. for the body speed and 4-wheel speeds of the MFC, Fig.12. for the slip ratio, and Fig.13. for the driving force vs. slip ratio of the front left wheel. The vehicle body speed and 4-wheel speeds of the MDFC are shown in Fig.14., the slip ratio in Fig.15. and the driving force vs. slip ratio of the left front wheel in Fig.16. From Fig. 8, 11, and 14, it can be seen that the wheel speeds of the 4-wheels significantly exceed the vehicle body speed in the constant torque control. In this simulation, all four wheels are on the low-friction road surface, so there is almost no difference between 4-wheel speeds in the case

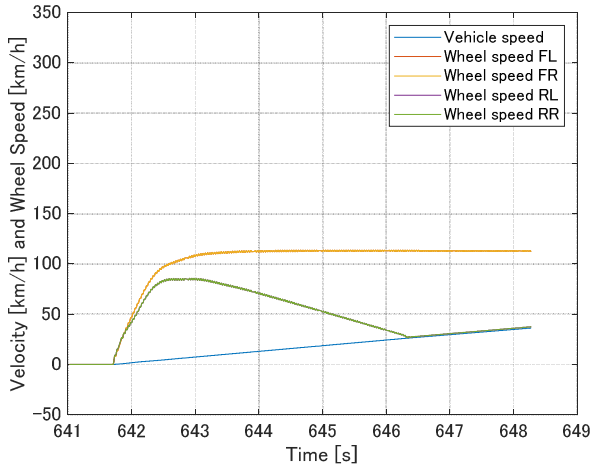

Fig.8. the vehicle body speed and 4-wheel speeds (Constant torque control)

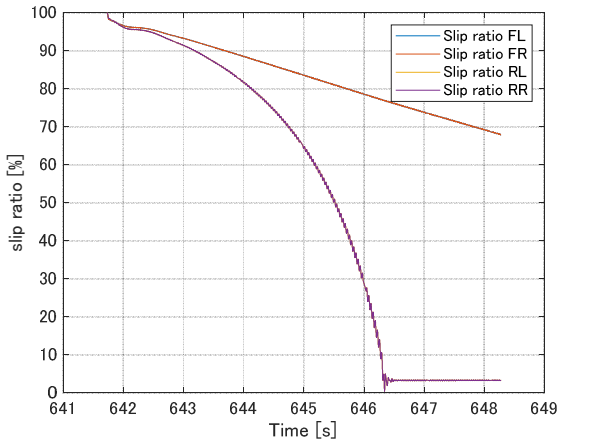

Fig.9. the slip ratio (Constant torque control)

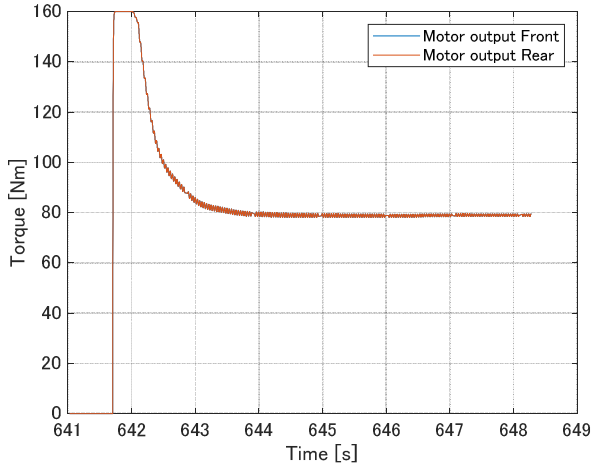

Fig.10. Constant torque control motor output (Constant torque control)

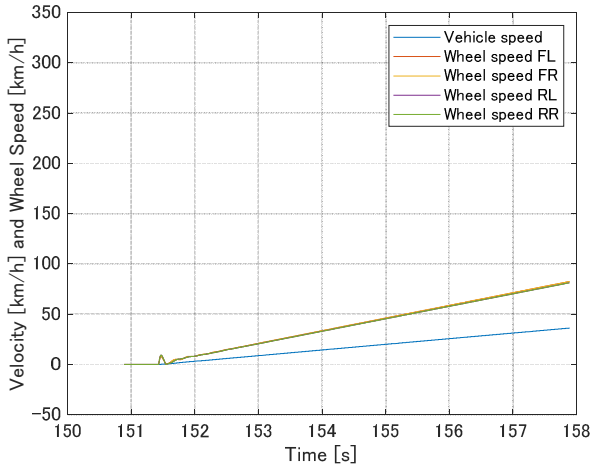

Fig.11. the vehicle body speed and 4-wheel Speeds (MFC)

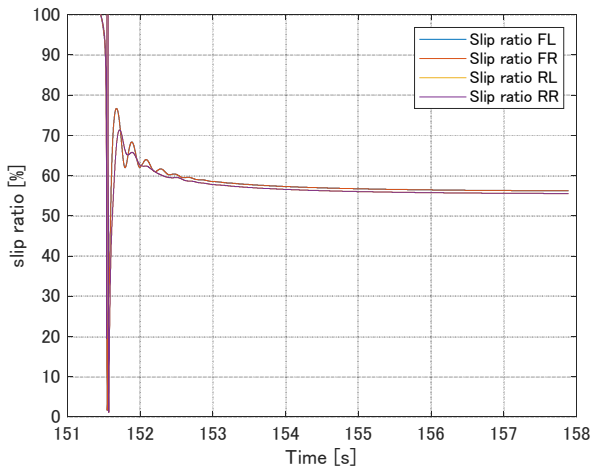

Fig.12. the slip ratio (MFC)

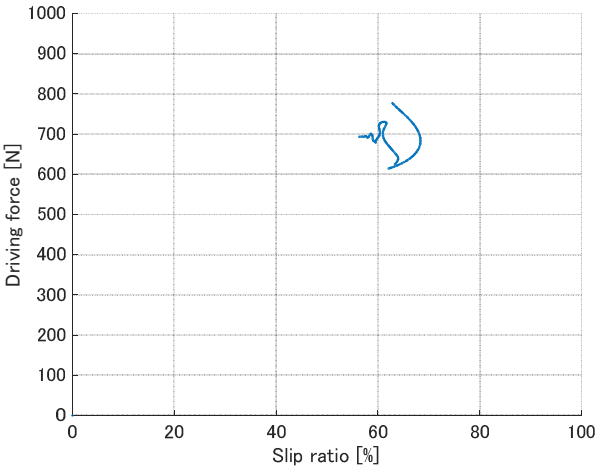

Fig.13. the driving force vs. slip ratio of the left front wheel (MFC)

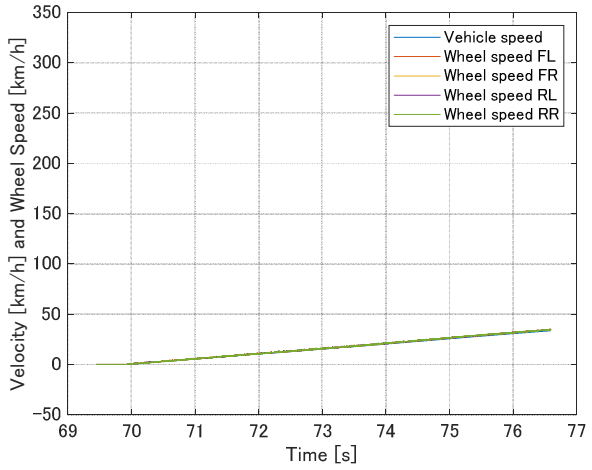

Fig.14. the vehicle body speed and 4-wheel speeds (MDFC)

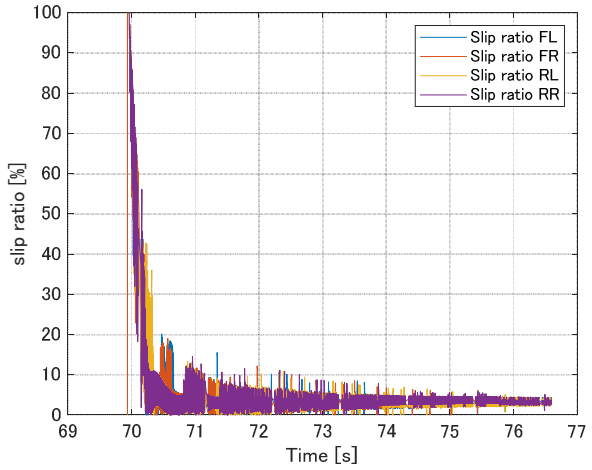

Fig.15. slip ratio (MDFC)

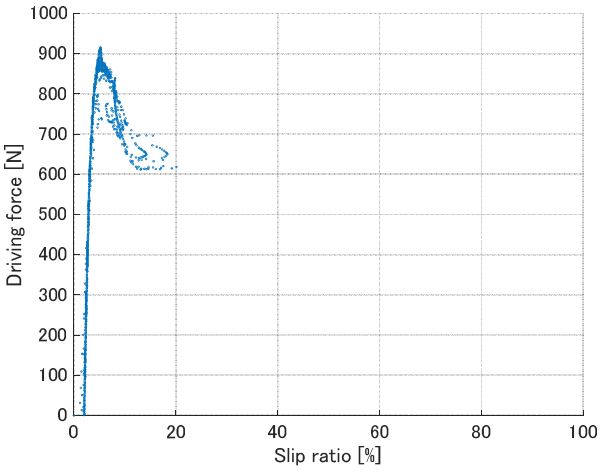

Fig.16. the driving force vs. slip ratio of the left front wheel (MDFC)

of four-wheel independent drive. In the case of front-rear independent drive, the difference occurred only in the front and rear wheels. In contrast, MDFC is able to suppress wheel slip, and there is no reduction in body speed due to control. In the constant torque control, only the rear wheels shifted to a non-spinning state. As shown in Fig. 10, this is caused by the torque characteristic of the motor, which decreases the torque when the wheel speed greatly exceeds the vehicle body speed during slip. In addition, the load shift to the rear during vehicle acceleration makes it easier to shift to the non-spinning state. Next, Fig.9 and 12 show that MFC has a lower slip rate than constant torque control. To reduce slip using MFC, the gain tuning of MFC is necessary. Fig.13 and 16 show that in MFC, the driving force points are concentrated on the right side of the figure, whereas in MDFC, the points are concentrated where the slip ratio is smaller than the maximum driving force point. This indicates that the MDFC is able to suppress the wheel slip well starting from the low-friction surface.

III. Conclusions

In conclusion, a driving simulator was constructed to perform vehicle driving tests in a virtual space. In the driving simulator, Simulation models for two-types of electric vehicle drive systems were designed. As a result of the simulation it was confirmed that MDFC suppressed wheel slip ratio better than the conventional constant torque control with independent drive of the front and rear wheels when driving on icy road surfaces. This is because the MDFC can independently output torque to each wheel to maintain the maximum driving force at each wheel, resulting in better traction performance. As next study, the design method for the parameters used in MDFC will be studied.

References

[1] Institute for Traffic Accident Research and Data Analysis,: https://www.itarda.or.jp/english/ (2021)

[2] Wen-Po Chiang, Dejun Yin, Manabu Omae, Hiroshi Shimizu: “Integrated Slip-Based Torque Control of Antilock Braking System for In-Wheel Motor Electric Vehicle”, IEEJ Journal of Industry Applications, Vol. 3, No. 4, pp. 318-327 (2014)

[3] Tomoki Emmei, Hiroshi Fujimoto: “Force Control of In-Wheel-Motored Electric Vehicles−Hand-Assisted Position Adjustment Based on Impedance Control—”, IEEJ Journal of Industry Applications, Vol. 9, No. 4, pp. 384-391 (2020).

[4] Y. Hori, Y. Toyoda, and Y. Tsuruoka: “Traction control of electric vehicle: basic experimental results using the test EV “UOT electric march””, IEEE Transactions on Industry Applications, Vol. 34, Vo. 5, pp. 1131-1138 (1998)

[5] Y. Hori, Y. Toyoda, and Y. Tsuruoka: “Traction control of electric vehicle based on the estimation of road surface condition-basic experimental results using the test EV “UOT electric march””, Proc. Power Conversion Conference-PCC '97, Vol. 1, pp. 1-8 (1997)

[6] K.Yoshimoto, T.Hanyu: “NISSAN e-POWER: 100 % Electric Drive and Its Powertrain Control”, IEEJ

Journal of Industry Applications, Vol. 10, No. 4, pp. 411-416 (2021).
[7] Maruzen Co.,Ltd: “Electric Automotive Handbook”, pp. 415-416 (2001)
[8] Y.Tsuruoka, Y.Toyoda, and Y.Hori:“Traction control of electric vehicle: basic experimental results using the test EV "UOT electric march"”, IEEE Transactions on Industry Applications, Vol. 34, No. 5, pp.1131-1138 (1998)
[9] A.Kawamura, K.Takeuchi, T.Furuya, M.Cao, Y.Takaoka, and K.Yoshimoto:“Measurement of Tractive Force and the New Maximum Tractive Force Control by the Newly Developed Tractive Force Measurement Equipment”, IEEJ Transactions on Industry Applications, Vol. 123, No. 8, pp.885-893 (2003)
[10] A.Kawamura, K.Takeuchi, T.Furuya, M.Cao, Y.Takaoka, and K.Yoshimoto:“Maximum Adhesion Control for Shinkansen using the Tractive Force Tester”, IEEE 28th Annual Conference of the Industrial Electronics Society, Vol. 1, pp. 567-572 (2002)
[11] K. Horikoshi, K. Yoshimoto and T. Yokoyama, "A Novel Maximum Adhesive Force Control without Vehicle Speed Sensor," 2022 International Power Electronics Conference (IPEC-Himeji 2022- ECCE Asia), Himeji, Japan, pp. 1873-1877 (2022)